Synthesis and Characterization of Chitosan-Starch as Electrolyte with MWNTs Reinforced for Lithium Batteries

Y. Estévez-Martínez[1,2], C. Guzmán-Martínez[2], D. Alaníz-Lumbreras[3], M. Mendoza-Duarte[4], V.M. Castaño[5], S.M. Durón-Torres[2],*.

[1]Nano Coating Technologies SA de CV, Paseo de las Palmas 555, Miguel Hidalgo, Distrito Federal, México, 11000.
[2]U. A. Cs. Químicas, Universidad Autónoma de Zacatecas, CU Siglo XXI Edificio 6, Km 6 Carr. Zac-Gdl, Zacatecas, Zac., México, 96160.
[3]Fac. de Ing. Eléctrica, Universidad Autónoma de Zacatecas, Avenida Ramón López Velarde No. 801, Zacatecas, Zac., México, 98000.
[4]Centro de Investigación en Materiales Avanzados CIMAV, Ave. Miguel de Cervantes 120, Chihuahua, Chih., México, 31109.
[5]Centro de Física Alicada y Tecnología Avanzada, Universidad Nacional Autónoma de México, Blvd. Juriquilla 3001, Querétaro, Qro., México, 76230.
*Tel.: +524929256690 ext 4655, duronsm@prodigy.net.mx

ABSTRACT

In recent years it has been reported that solid electrolytes may be considered promising materials for storing energy, due to their unique properties, such as high ionic conductivity, physical flexibility and their ability to provide good electrode / electrolyte contact. Compared to the liquid state, the production of leak and gas formation during the decomposition of the solvent is avoided, in addition to being compact, lightweight and safe.

In this work is reported the synthesis and the physical and electrochemical characterization of chitosan-starch polymers modified with carbon nanotubes and lithium. The structural and physicochemical properties of the polymers were characterized by Dynamical Mechanical Analysis, FTIR and Raman spectroscopy. The electrical and electrochemical properties were then determined by using Electrochemical Impedance Spectroscopy and Conductivity Measurements. The results obtained indicate that the polymeric material is a viable candidate to be used as electrolyte for lithium batteries.

Keywords: Nanocomposite-Biopolymer; Electrolyte; Lithium Batteries.

1. Introduction.

A polymer electrolyte can be defined as a membrane having transport properties comparable with those of common ionic liquids solutions [1]. The electrolyte is the heart of a cell which separates the electrodes upon the occurrence of an electrochemical reaction through the conduct of an ion in specific from one electrode to another at high operating speeds in the cell, where transport should be fast and highly selective, but these properties are often in conflict with each other. Proton conductive materials are used as electrolyte fuel cells of low and medium temperature and are attracting great interest [2]. That is, the high ionic conductivity requires an electrolyte, but is often inversely proportional to its mechanical strength. This represents a challenging paradigm for the design of new multifunctional materials focused on engineering [3]. Complexes between lithium salt form classic examples used as electrolyte membranes, LiX, $LiClO_4$ or $LiN(CF_3SO_2)_2$ and a high molecular weight polymer containing groups coordinated with Li^+. Examples of these polymers are: poly (ethylene oxide), poly (propylene oxide) poly (bis (methoxy ethoxyethoxide)-phosphazene), poly (dimethyl siloxane), poly (acrylonitrile), poly (methyl methacrylate), poly (vinyl chloride) and poly (vinylidene fluoride) [1,4]. All polymers referred above relate to monomeric chains that are difficult to degrade, causing a big problem of pollution to environment. For these reason it has been great interest to perform research on natural polymers (carbohydrates) that by their nature are naturally degraded to a certain time. Such polymers are commonly called biopolymers.

These biopolymers, according to a review on the use of these polymers as electrolytes a like to cellulose, starch, chitosan, agar, pectin and gelatin were used [5]. However, the use of chitosan an starch were studied for different authors [6–15], where the properties and characteristics are explained in detail, but only some papers have published their use as matrix in the carbon nanotube reinforcement[9,16–18], but the most important is know the use of the biopolymer like to electrolyte, where its use is currently very fertile field of research forward [5,19–22].

2. Experimental.

Multiwalled carbon nanotubes (MWNTs) were obtained from Sun Nanotech Co., which produced them by chemical vapor deposition, with a diameter from 10 to 30 nm and 1 to 10 μm long, with a purity >90% and surface area of 90 to 350 m^2/g[23]. The other reactive were purchased from Sigma-Aldrich Co. LLC., and used without further purification.

Based on previous reports [24–29], the purification/oxidation of the MWNTs was achieved in liquid phase with a 3:1 mix of NHO_3 (95%) and H_2SO_4 (98%) at 85º C for 3 h in a reflow process. The resulting material was vacuum-washed to a neutral pH with deionized water. For the lithiated-nanotubes, according to a report by The Naval Academy, Annapolis [30], the following method is proposed: 25 ml at 6:1 w/w MWOHs to LiOH were mixed and reacted at reflux to 75º C by 2h (RLi) and sonicated by 2 h (SLi), respectively. On the other hand, according to previous research [7,10,22,31–34], experimental methodology suggested for the synthesis of starch-chitosan film (ChSt) to 1:1 at 2% m/v: the chitosan solution (2% m / v) was prepared by dispersing 2 g of chitosan in 100 ml of acetic acid solution (1% v / v), then stirred mechanically at 100 rpm. After the chitosan is completely dispersed, sonicated for 15 minutes to break any air bubbles present, then allowed stand until homogenous solution. The aqueous starch solution (2% m/v) was prepared by heating above its gelatinization temperature[35], of 90 ± 2° C

by 20 min with mechanical stirring. During this time, the glycerin (1% v/v) was added to final cooling to room temperature with mechanical stirring. The films were dried chitosan-starch deposited on a polystyrene mold at room temperature in an extraction hood for 24 h. After this time, the corresponding characterizations were made. To reinforce the electrolyte: MWNTs (ChStMW), MWOHs (ChStOH), lithiated-nanotubes by reflux (ChStRLi) and sonicated (ChStSLi) were used with a 0.025% w/v with at biopolymer respect.

Infrared (FTIR) spectra were recorded in a Vector 33 Bruker spectrophotometer at 32 scans, with a resolution of 4 cm^{-1}. Solid samples were embedded in KBr disks. Raman spectra were recorded in a Micro-Raman Dilor with a resolution of 515 cm^{-1}, with a 514.5 nm laser with 15 s of integration time. The analyses X-ray Photoelectron Spectrometer (XPS) were performed with a JPS-9200 Photoelectron Spectrometer (ESCA). Dynamic mechanical analysis (DMA) were recorded in a TA instruments, RSA III model, were run using tweezers to tension in a temperature range from 30 ° C to 350 ° C. In all the samples using a frequency of 1.0 Hz. The electrical conductivity of the membranes was measured by a standard four-probe method on a milliohm-meter (Agilent 4338B Milliohm Meter 1kHz) at room temperature, where the equipment was calibrated with platinum and gold pure that knowing the theoretical resistivity of the two materials ($10.6x10^{-8}$ Ωm and $2.44x10^{-8}$ Ωm respectively [36]), a geometric factor was obtained (1.063 a.u.).

. The electrochemical measurements were performed using an EG&G PAR VersaSTAT 3 Potentiostat/Galvanostat, where electrochemical impedance spectroscopy (EIS) experiments were carried out in the potentiostatic mode in the 1 MHz to 1Hz frequency range. The impedance spectra were registered with a logarithmic data collection scheme at 10 steps per decade at the open-circuit potential (0.22 V) with alternate signal amplitude of 10 mV.

3. Results and discussion.

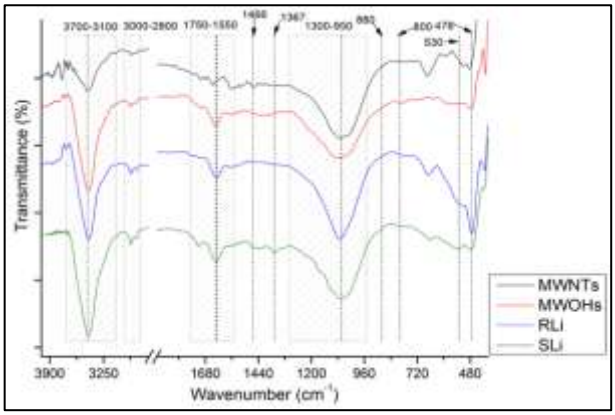

Figure 01. FTIR of nanotubes oxidized and lithiated.

Regardless of the characteristic FTIR peaks of the carbon nanotubes, that describe at normal modes of vibration at ~1632 cm^{-1} for E_{1u} and ~800 cm^{-1} for A_{2u} in multiwall carbon nanotubes (MWNTs), confirmed by different authors[37–41] and increases in other bands that identify in the oxidation of

multiwall oxidized carbon nanotubes (MWOHs) as between 1750—1550 cm^{-1} for ν(C=O), 1466 cm^{-1} for δ(O-H) and between 1300—950 cm^{-1} for ν(C-O) due to vibrations of the carboxyl groups, 3443 cm^{-1} for isolated surfaces of ν_s(OH)[41–44], the presence of lithium in the samples, was measured according to the interaction with the oxygen and carbon to generate electrostatic bonds with the metal, thus, according with some authors[45–50], The molecular vibration bands, suggest the presence of $ROCO_2Li$, Li_2O, Li_2CO_3, ROLi and LiOH are appreciated. For lithium hydroxide, is visible the O-H band at 3700-3100 cm^{-1}, these bands are broader than MWOHs for the same range of wave number. For st(C-H) at 3000-2800 cm^{-1} and st(C-O) at 1064 cm^{-1}, corresponding to $ROCO_2Li$ and ROLi respectively, where st(Li-O) of the Li_2O is visible at 530 and 476 cm^{-1} too. In addition, the C-O band at 880 cm^{-1} of the Li_2CO_3, is caused by the intensity strong of the band like an arm weak. Finally, the bending vibrations CH_2 at 1466 cm^{-1} and C=O like a symmetric at 1628 cm^{-1} and asymmetric at 1367 cm^{-1} vibrations, indicate the presence of $ROCO_2Li$. In the Figure 01 shows the comparative, where all the vibrations of the nanotubes with lithium are present.

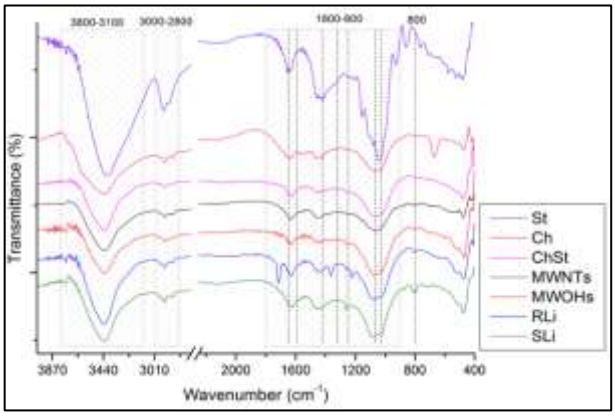

Figure 02. FTIR of starch (St), chitosan (Ch) and chitosan-starch (ChSt). ChSt are reinforced with nanotubes oxidized and lithiated.

For the nanocomposites Chitosan-Starch as matrix and with different reinforcements (Carbon nanotubes with lithium), the FTIR spectrum is presented in Figure 02. For starch at 3274 cm^{-1} the st(O-H) of the glycosidic chains, are present. Addition to this band, at 2921 y 2926 cm^{-1} is because the st(CH) are associated with the ring methine hydrogen atoms [14,51–53]. For chitosan, at 3496 cm^{-1} is due to OH group (ν_{OH}), at 3345 cm^{-1} is due to NH group-stretching vibration (ν_{NH}), at 2926, 2873, 1421, 1322 and 1249 cm^{-1} is due to symmetric or asymmetric CH_2 stretching vibration attributed to pyranose ring (ν_{CH}), at 1646 cm^{-1} is due to C=O in amide groups (amide I band), at 1593 cm^{-1} is due to NH_2 bending vibration in amino group (δ_{NH2}), at 1421 and 1322 cm^{-1} is due to vibrations of OH, CH in the ring, at 1381 cm^{-1} is due to CH_3 in amide group, at 1249 cm^{-1} is due to C—O group, 1156 cm^{-1} is due to —C—O—C— in glycosidic linkage, 1096 and 1030 cm^{-1} is due to C—O group ($\nu_{C—O}$) in amide group and, 897 cm^{-1} is due to CH_3COH group, are presents [54–56]. When mixing both polymers (Chitosan-Starch), there is a widening with respect to chitosan in the OH band due to the presence of starch, in addition to amide and amines groups, which characterize the chitosan [14,34,52,53]. Due to the very low concentration reinforcement in the matrix, the characteristics bands of carbon nanotubes with lithium are very weak,

however, come to appreciate some of them, like those that have been described to be characterized and discussed by this technique.

The Raman spectroscopy was used to characterize MWNTs, MWOHs and lithiated-nanotubes (RLi and SLi), where the graphic shows in the Figure 03 and tabulated in the same Figure. For many authors, Raman spectroscopy is considered as the fingerprint of carbon nanotubes[57–63], that's why is very important make a deep analysis on the oxidation, purification and modification in the structure of the outer walls of carbon nanotubes. In Raman spectroscopy, the peaks to ~1570 cm^{-1} (G band), ~1340 cm^{-1} (D band) and ~2684 cm^{-1} (G' band) were studied and have been analyzed by different authors [43,61,63–72]. To verify the oxidation/purification of the multiwall carbon nanotubes (from MWNTs to MWOHs), some publications [73,74] consider the G band (≈1590 cm^{-1}) as an indicator of purity due to the excellent graphitic orientation that this represents in the carbonaceous materials by its sp^2 hybridization, free of broken links or other hybridizations present including sp^3, however, other papers[75,76], they evaluate the purity of carbon nanotubes with the D band (≈1350 cm^{-1}), because it is sensitive to the carbonaceous impurities and structural defects in the graphitic sp^2 networks samples (this contrary to the G band), therefore, we can conclude that the relationship between the intensities of these two bands is related to the purity of carbon nanotubes, but with the disadvantage, according to Anne C. Dillon[76], that only not the intensity is important, the full-width-at-half-maximum (FWHM) of the D band is much broader than that of the nanotube D-band, from 86 cm^{-1} a 57 cm^{-1} of graphite to 42cm^{-1} a 17 cm^{-1} of carbon nanotubes. The G' band, according to Roberta A. DiLeo[77], its intensity is proportional to the purity of the multiwall carbon nanotubes due to the absence of nano-carbons (disordered phase) in the samples. For all the reasons described above, in this work, we related the areas of the G'/G, G'/D and D/G bands to find a relationship purity of carbonaceous material and presence of intercalated lithium. The dimensionless values areas of G, D and G' bands and the relationship of them, suggest the carbonaceous purification of MWNTs at the oxidation with acids MWOHs due to the decrease in the ratio D/G and the increase in the ratio G'/D and low difference G'/G by the removal of carbonaceous material.

Sample	D	G	G'	G'/G	G'/D	D/G
MWNTs	72,068	79,955	81,314	1.02	1.13	0.90
MWOHS	40,546	52,738	51,791	0.98	1.28	0.77
RLi	64,666	80,951	77,683	0.96	1.20	0.80
SLi	98,968	117,520	108,288	0.92	1.09	0.84

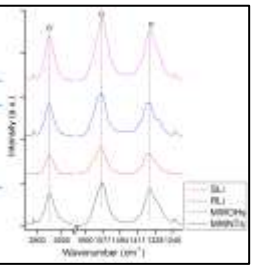

Figure 03. Raman spectroscopy of nanotubes oxidized and lithiated with the relationship of the characteristic area bands of nanotubes oxidized and lithiated in Raman.

For the samples intercalated with lithium show a drop in G'/D regarding oxidized nanotubes due to the increased area of the G' band because of the exfoliating action through basic lithium hydroxide which degrades carbonaceous materials[78,79], making more active nanotubes walls[80] but that also increases the band D for the lithium intercalated in the walls that in the center of the tube that is less favorable because of the strong core repulse between Li ions and carbon inner walls[81]. Furthermore, the

most important is the significant increase of the G, band that could be assigned to the lithiated carbon nanotubes, according to various publications [81–88].

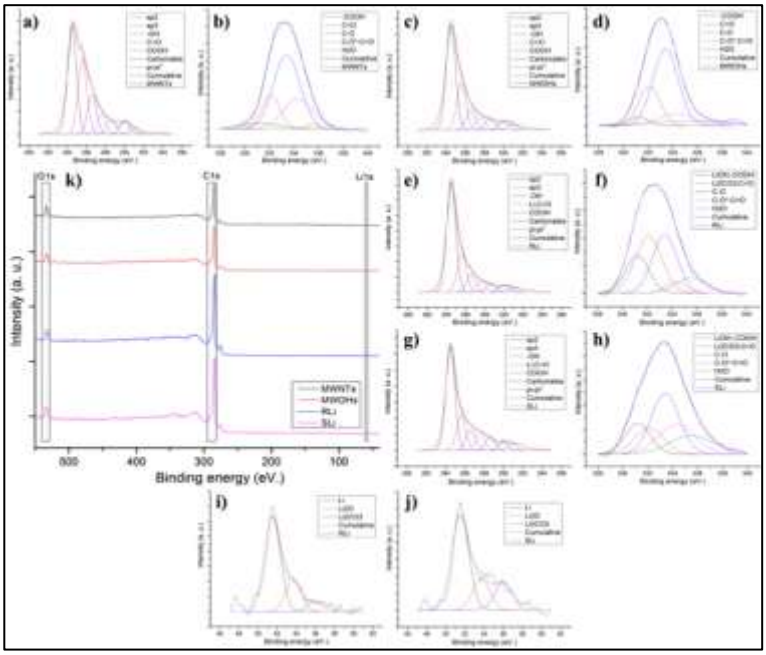

Figure 04. XPS of MWNTs, MWOH, RLi and SLi samples of C_{1s} (a), c), e) and g) respectively), O_{1s} (b), d), f) and h) respectively) and Li_{1s} in i) and j) of RLi and SLi, respectively.

X-ray photoelectron spectroscopy was used for quantify the lithium on multiwall oxidized carbon nanotubes with respect to carbon and oxygen. Binding energy ranges for carbon (C1s) at 295-281 eV, oxygen (O1s) at 540-528 eV and lithium (Li1s) at 61-57 eV were evaluated. For C1s and O1s there are different focus to determine the energy levels in which the molecules related to these two elements can occur. The deconvolution of C1s, O1s and Li1s peaks [48,89–92]. C1s peak at 284.5 eV shows sp2 hybridization for CH_3OLi, at 285.6 eV shows sp3 hybridization for CH_3CH_2OLi, at 286.6 eV shows the hydroxyl groups of oxidized carbon nanotubes with not relation with lithium, at 287.6 eV for carbonyl C=O in CH_3OCO_2Li, at 288.6 eV shows the carboxyl groups —COOH of oxidized carbon nanotubes with not relation with lithium, at 290 eV shows lithium carbonate and finally, at 290.9 eV shows electronic transitions π-π* with not relation with lithium but is a characteristic special in the walls of carbon nanotubes. O1s peak at 531.2, 532.1, 533.4, 534.3 and 535.5 eV correspond to LiOH, O=C of Li_2CO_3, O—C of $ROCO_2Li$, C—O*-C=O and H_2O respectively. Li1s peak at 51.5 eV and 53.7 eV for Li_2O and at 56 eV for lithium carbonate (Li_2CO_3). The Figure 04 shows the percent of deconvolution in each band. In C1s, the hydroxyl (—OH at 286.6 eV) and carboxyl (—COOH at 288.6 eV) band of lithiated nanotubes are higher than oxidized nanotubes, thus as the carbonate band (290.0 eV) probably to lithium carbonate on nanotube walls. The increase of the electronic transitions (π-π* at 290.9 eV) in oxidized carbon nanotubes suggests that there is to exfoliation walls due to acids[41], however, there is a decrease in the lithiated nanotubes suggests a non covalent interaction among them. Removing carbonaceous material is reflected in the hybridization of the carbon atoms of the nanotubes (sp^2 at 284.5 eV and sp^3 at 285.6 eV),

reflecting the same behavior as G and D bands Raman. In O1s, according is oxidized and lithium intercalates in the walls of carbon nanotubes, carboxyl, carbonyl and carbonate bands (—COOH at 531.2 eV, O=C at 532.1 eV and C—O*—C=O at 534.3 eV) increases. The carbonate is confirmed in Li1s (Li2CO3 at 56 eV), however, the greater amount of lithium is manifested as a strong electrostatic interaction of lithium ions due to a decrease in the peak transitions in C1s (π-π* at 290.9 eV) and the increase in lithium ions band (51.5 eV)[89].

Scanning electronic microscopy (SEM) and dynamic mechanical analysis (DMA), were used to characterize at the electrolyte with MWNTs and MWOHs as reinforcement, since the purpose of these characterizations, it is to know the ability of carbon nanotubes in the polymeric matrix for scattering, regardless of the lithiation of the carbon nanotubes. DMA can be categorized as a thermo-mechanical test because data are obtained corresponding to the viscoelastic nature of the material at different temperatures. Some of the general purpose DMA are determine the storage modulus and heat dissipation of viscoelastic materials over time spectrum (frequency) by temperature and strain, detecting transitions and change variables associated with each other in the viscoelastic properties to relate structure—property [93,94].

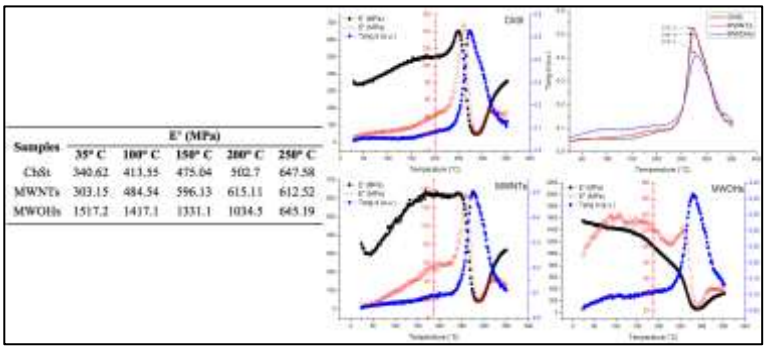

Samples	E' (MPa)				
	35° C	100° C	150° C	200° C	250° C
ChSt	340.62	413.55	475.04	502.7	647.58
MWNTs	303.15	484.54	596.13	615.11	612.52
MWOHs	1517.2	1417.1	1331.1	1034.5	645.19

Figure 05. DMA of ChSt and nanocomposites reinforced with MWNTs and MWOHs. Also, the elastic modulus at different temperatures tabulated.

The graph of the elastic modulus E', the material ability to store energy was evaluated at five different temperatures (35°, 100°, 150°, 200°, and 250° C) where the samples have a viscoelastic behavior to its degradation. The results are tabulated and showed in Figure 05, where is visible the ability of the MWOHs for increase the elastic modulus up to 445.4% to 35ºC, where still 200º C the elastic module up to 205.8% grater than with respect to the original matrix of chitosan-starch. With MWNTs, the elastic modulus of material is practically the same.

The loss modulus (E") related to the liquid-like, reflecting the viscous behavior of the nanocomposite and the glass transition temperature of the material (tg), where in the same Figure 05 is evident the increase of the chitosan-starch film with multiwall oxidized carbon nanotubes reinforcement. Here is possible to view a null activity of MWNTs in the biopolymer matrix.

In the nanocomposite, the energy dissipation is manifested as an internal friction of the material, where a friction between the reinforcement and the matrix is developed. The internal friction can be

determined by the relationship between the loss and stored energy, known as tangent delta. The amount of internal energy dissipated in the interface depends on the degree of adhesion between the phases, where an adhesion charge/weak matrix promotes high internal friction which is reflected in higher values of delta tangent (Tang δ).

With Tang δ, suggest that the nanocomposite with MWNTs as reinforcement does not show a significant difference in the coefficient of dispersion, however, to oxidize (MWOHs) have a lower coefficient of dispersion. This infers that has a good interface between the materials, since the internal friction between polymer chains has greatly decreased due to the hydrogen bonds generated between the functional groups of the carbon nanotubes with the amino and hydroxyl groups of the chitosan matrix-starch, which limits its mobility and, therefore, reduces its friction. Thus, not only nanotubes oxidized carbon help in the mechanical properties of the polymer, but also on its thermal properties, since the glass transition temperature is significantly increased from 272º C to 279º C, are 7° C improvement.

The electrical and ionic conductivity values are tabulated in the Figure 07. Is possible see that the electrical conductivity is affected by the reinforcement of the MWNTs and MWOHs, however, with the lithiated carbon nanotubes, the increase is insignificant, considering that there is a relationship 6:1 w/w of MWOHs with respect to LiOH and only there is a reinforcement of 0.025% m/v with respect to biopolymer. Perhaps electrical conductivity could be considered low, however, when compared with similar results, for example the use of reinforced polyaniline (semiconducting polymer) with amidized multiwall carbon nanotubes, one can see values of 0.73 S/m with relationship 1:120 of multiwall carbon nanotubes with respect to monomer[95]. For Starch–NH_4NO_3 electrolyte, was reported a conductivity of 0.00283 S/m at room temperature[96].

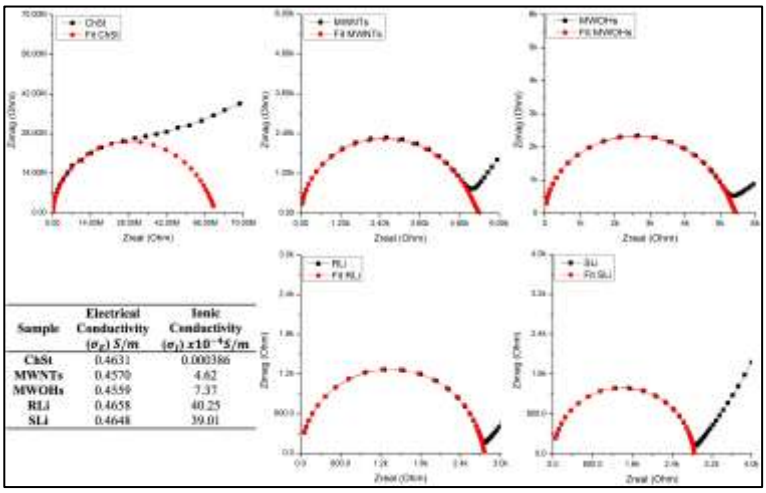

Sample	Electrical Conductivity (σ_e) S/m	Ionic Conductivity (σ_i) x10^{-4}S/m
ChSt	0.4631	0.000386
MWNTs	0.4570	4.62
MWOHs	0.4559	7.37
RLi	0.4658	40.25
SLi	0.4648	39.01

Figure 07. Nyquist plot of the membrane samples with fitted by trial and error, where is obtained R_b. Also, the electrical and ionic conductivity of the samples are showed in the same figure.

For the calculation of the ionic conductivity, the impedance spectroscopy has been widely used to characterize the nature of lithium-ion electrode processes and interfacial properties, as well as for

distinguishing individual contributions to overall cell impedance and resistivity[97,98]. From the impedance plot in the Nyquist format, the bulk resistance, R_b can be obtained at minimum Z_{im} obtained by trial and error until the experimental plot is fitted and the ionic conductivity can be calculated by substituting R_b into the equation below: $\sigma = l/(R_b A)$ where σ is the ionic conductivity, R_b is the bulk resistance, l is the thickness of the pellet and A is the cross sectional area. The bulk resistance was calculated from the high frequency intercept on the real impedance axis of the Nyquist plot[22] demonstrated in the Figure 07.

Is visible the decreasing the semicircle to be reinforced with carbon nanotubes MWNTs and MWOHs, however, with carbon lithiated nanotubes, RLi and SLi, the bulk resistance value is less. When the resistance value decreases accordingly, thus the conductivity increases when considering the cross-sectional area and thickness of the samples are considered. The prolongation of the semicircles of Nyquist plot is plotted in Figure 07. At know the ionic conductivity values of the samples, is easy to distinguish the increase of its conductivity at reinforced with carbon nanotubes, but mainly carbon lithiated nanotubes, ranging from 0.000386 to 40.25 x 10^{-4} S/m.

4. Summary and perspectives.

Conjunction with the different XPS, FTIR and Raman spectroscopies, the carbon lithiated and oxidized nanotubes were confirmed, where the interaction of the OH of LiOH are bonded with the different groups of hydroxyls and carbonyls of oxidized nanotubes is satisfactory. For scanning electros microscopy and dynamic-mechanical analysis, the MWNTs and MWOHs behavior was studied on the biopolymer ChSt matrix, where is visible the capacity of this nanostructured of improve their mechanical properties, but are the carbon lithiated nanotubes (RLi and SLi) where the electrical and ionic conductivity are enhanced, mainly its high ionic conductivity that helps propose it as an electrolyte battery.

Acknowledgments.

The authors are indebted to Dr. Genoveva Hernández-Padrón, Mrs. Carmen Vazquez, and Mrs. Alejandra Núñez Pineda of Universidad Nacional Autonoma de Mexico and Dr. Erick Cuevas Yañez and Gustavo López Téllez of Universidad Autonoma del Estado de Mexico for their technical support with the synthesis, FTIR, Raman and XPS studies. They thank the National Council of Science and Technology of Mexico (CONACyT) and FOMIX-CONACYT (ZAC-2010-C04-149908) for their financial support.

References.

[1] F. Croce, R. Curini, A. Martinelli, L. Persi, F. Ronci, B. Scrosati, et al., Physical and chemical properties of nanocomposite polymer electrolytes, J. Phys. Chem. B. 103 (1999) 10632–10638.

[2] E.L. Chávez, R. Oviedo-Roa, G. Contreras-Pérez, J.M. Martínez-Magadán, F.L. Castillo-Alvarado, Theoretical studies of ionic conductivity of crosslinked chitosan membranes, Int. J. Hydrog. Energy. 35 (2010) 12141–12146.

[3] P. Liu, E. Sherman, A. Jacobsen, Design and fabrication of multifunctional structural batteries, J. Power Sources. 189 (2009) 646–650.

[4] J.Y. Song, Y.Y. Wang, C.C. Wan, Review of gel-type polymer electrolytes for lithium-ion batteries, J. Power Sources. 77 (1999) 183–197.

[5] P.K. Varshney, S. Gupta, Natural polymer-based electrolytes for electrochemical devices: a review, Ionics. 17 (2011) 479–483.

[6] M.B. Vásconez, S.K. Flores, C.A. Campos, J. Alvarado, L.N. Gerschenson, Antimicrobial activity and physical properties of chitosan–tapioca starch based edible films and coatings, Food Res. Int. 42 (2009) 762–769.

[7] F.M. Pelissari, M.V. Grossmann, F. Yamashita, E.A.G. Pineda, Antimicrobial, mechanical, and barrier properties of cassava starch–

chitosan films incorporated with oregano essential oil, J. Agric. Food Chem. 57 (2009) 7499–7504.
[8] Y.X. Xu, K.M. Kim, M.A. Hanna, D. Nag, Chitosan–starch composite film: preparation and characterization, Ind. Crops Prod. 21 (2005) 185–192.
[9] K.Y. Castrejón-Parga, H. Camacho-Montes, C.A. Rodríguez-González, C. Velasco-Santos, A.L. Martínez-Hernández, D. Bueno-Jaquez, et al., Chitosan–starch film reinforced with magnetite-decorated carbon nanotubes, J. Alloys Compd. (2014).
[10] S. Chillo, S. Flores, M. Mastromatteo, A. Conte, L. Gerschenson, M.A. Del Nobile, Influence of glycerol and chitosan on tapioca starch-based edible film properties, J. Food Eng. 88 (2008) 159–168.
[11] M.A. Garcia, A. Pinotti, N.E. Zaritzky, Physicochemical, water vapor barrier and mechanical properties of corn starch and chitosan composite films, Starch- Stärke. 58 (2006) 453–463.
[12] H. Liu, R. Adhikari, Q. Guo, B. Adhikari, Preparation and characterization of glycerol plasticized (high-amylose) starch–chitosan films, J. Food Eng. 116 (2013) 588–597.
[13] C. Bangyekan, D. Aht-Ong, K. Srikulkit, Preparation and properties evaluation of chitosan-coated cassava starch films, Carbohydr. Polym. 63 (2006) 61–71.
[14] T. Bourtoom, M.S. Chinnan, Preparation and properties of rice starch-chitosan blend biodegradable film, LWT - Food Sci. Technol. 41 (2008) 1633–1641.
[15] A. Lazaridou, C.G. Biliaderis, Thermophysical properties of chitosan, chitosan–starch and chitosan–pullulan films near the glass transition, Carbohydr. Polym. 48 (2002) 179–190.
[16] L. Yan, P.R. Chang, P. Zheng, Preparation and characterization of starch-grafted multiwall carbon nanotube composites, Carbohydr. Polym. 84 (2011) 1378–1383.
[17] M.V. Deepthi, G.S. Ananthapadmanabha, P. Sampathkumaran, S. Seetharamu, V.V. Pattenshetti, S. Ganga, et al., Preparation of bio-nanocomposites of chitosan/thermoplastic starch reinforced with multiwalled carbon nanotubes, in: Prop. Appl. Dielectr. Mater. ICPADM 2012 IEEE 10th Int. Conf. On, IEEE, 2012: pp. 1–4.
[18] F. Xie, E. Pollet, P.J. Halley, L. Averous, Starch-based nano-biocomposites, Prog. Polym. Sci. 38 (2013) 1590–1628.
[19] Y.M. Yusof, M.F. Shukur, H.A. Illias, M.F.Z. Kadir, Conductivity and electrical properties of corn starch–chitosan blend biopolymer electrolyte incorporated with ammonium iodide, Phys. Scr. 89 (2014) 035701.
[20] M.F. Shukur, N.A. Majid, R. Ithnin, M.F.Z. Kadir, Effect of plasticization on the conductivity and dielectric properties of starch–chitosan blend biopolymer electrolytes infused with NH4Br, Phys. Scr. 2013 (2013) 014051.
[21] M.F. Shukur, R. Ithnin, M.F.Z. Kadir, Electrical properties of proton conducting solid biopolymer electrolytes based on starch–chitosan blend, Ionics. (2013) 1–23.
[22] Y.N. Sudhakar, M. Selvakumar, Lithium perchlorate doped plasticized chitosan and starch blend as biodegradable polymer electrolyte for supercapacitors, Electrochimica Acta. 78 (2012) 398–405.
[23] Sun, X., Zeng, X., Cheng, G., Sun Nanotech Company, Sun Nanotech Co Ltd. (2013). http://www.sunnano.com/.
[24] Z. Spitalsky, D. Tasis, K. Papagelis, C. Galiotis, Carbon nanotube–polymer composites: chemistry, processing, mechanical and electrical properties, Prog. Polym. Sci. 35 (2010) 357–401.
[25] S. Osswald, M. Havel, Y. Gogotsi, Monitoring oxidation of multiwalled carbon nanotubes by Raman spectroscopy, J. Raman Spectrosc. 38 (2007) 728–736.
[26] C.-E. Hong, J.-H. Lee, P. Kalappa, S.G. Advani, Effects of oxidative conditions on properties of multi-walled carbon nanotubes in polymer nanocomposites, Compos. Sci. Technol. 67 (2007) 1027–1034.
[27] H. Yu, Y. Jin, F. Peng, H. Wang, J. Yang, Kinetically controlled side-wall functionalization of carbon nanotubes by nitric acid oxidation, J. Phys. Chem. C. 112 (2008) 6758–6763.
[28] J. Zhang, H. Zou, Q. Qing, Y. Yang, Q. Li, Z. Liu, et al., Effect of chemical oxidation on the structure of single-walled carbon nanotubes, J. Phys. Chem. B. 107 (2003) 3712–3718.
[29] T.-C. Hung, C.-F. Chen, M. Chen, C.-C. Chen, Quantitative limitation of active site and characteristics of chemical oxidized well-aligned carbon nanotubes, Thin Solid Films. 516 (2008) 5236–5240.
[30] J.R. Jaunsen, The Behavior and Capabilities of Lithium Hydroxide Carbon Dioxide Scrubbers in a Deep Sea Environment., Naval Academy Annapolis MD, 1989.
[31] J. Ai, M. Rezaei-Tavirani, E. Biazar, K.S. Heidari, R. Jahandideh, Mechanical properties of chitosan-starch composite filled hydroxyapatite micro-and nanopowders, J. Nanomater. 2011 (2011) 16.
[32] M.O. Tuhin, N. Rahman, M.E. Haque, R.A. Khan, N.C. Dafader, R. Islam, et al., Modification of mechanical and thermal property of chitosan–starch blend films, Radiat. Phys. Chem. 81 (2012) 1659–1668.
[33] L. You, F. Lu, D. Li, Z. Qiao, Y. Yin, Preparation and flocculation properties of cationic starch/chitosan crosslinking-copolymer, J. Hazard. Mater. 172 (2009) 38–45.
[34] A. Espíndola-González, A.L. Martínez-Hernández, F. Fernández-Escobar, V.M. Castaño, W. Brostow, T. Datashvili, et al., Natural-Synthetic hybrid polymers developed via electrospinning: The effect of PET in chitosan/starch system, Int. J. Mol. Sci. 12 (2011) 1908–1920.
[35] H. Liu, L. Yu, K. Dean, G. Simon, E. Petinakis, L. Chen, Starch gelatinization under pressure studied by high pressure DSC, Carbohydr. Polym. 75 (2009) 395–400.
[36] Sigma-Aldrich Co. LLC., Sigma-Aldrich Co. LLC., MSDS Search Prod. Saf. Cent. (2014). http://www.sigmaaldrich.com/safety-center.html.
[37] T. Belin, F. Epron, Characterization methods of carbon nanotubes: a review, Mater. Sci. Eng. B. 119 (2005) 105–118.
[38] U. Kuhlmann, H. Jantoljak, N. Pfänder, P. Bernier, C. Journet, C. Thomsen, Infrared active phonons in single-walled carbon nanotubes,

Chem. Phys. Lett. 294 (1998) 237–240.
[39] A. Aqel, K.M. El-Nour, R.A. Ammar, A. Al-Warthan, Carbon nanotubes, science and technology part (I) structure, synthesis and characterisation, Arab. J. Chem. 5 (2012) 1–23.
[40] R.L. McCreery, Advanced carbon electrode materials for molecular electrochemistry, Chem Rev. 108 (2008) 2646–2687.
[41] Y. Estévez-Martínez, C. Velasco-Santos, A.-L. Martínez-Hernández, G. Delgado, E. Cuevas-Yáñez, D. Alaníz-Lumbreras, et al., Grafting of multiwalled carbon nanotubes with chicken feather keratin, J. Nanomater. 2013 (2013).
[42] L. Stobinski, B. Lesiak, L. Kövér, J. Tóth, S. Biniak, G. Trykowski, et al., Multiwall carbon nanotubes purification and oxidation by nitric acid studied by the FTIR and electron spectroscopy methods, J. Alloys Compd. 501 (2010) 77–84.
[43] J.H. Lehman, M. Terrones, E. Mansfield, K.E. Hurst, V. Meunier, Evaluating the characteristics of multiwall carbon nanotubes, Carbon. 49 (2011) 2581–2602.
[44] U. Kuhlmann, H. Jantoljak, N. Pfänder, P. Bernier, C. Journet, C. Thomsen, Infrared active phonons in single-walled carbon nanotubes, Chem. Phys. Lett. 294 (1998) 237–240.
[45] P. Verma, P. Maire, P. Novák, A review of the features and analyses of the solid electrolyte interphase in Li-ion batteries, Electrochimica Acta. 55 (2010) 6332–6341.
[46] C. Naudin, J.L. Bruneel, M. Chami, B. Desbat, J. Grondin, J.C. Lassègues, et al., Characterization of the lithium surface by infrared and Raman spectroscopies, J. Power Sources. 124 (2003) 518–525.
[47] M.A. Karakassides, D. Gournis, D. Petridis, An infrared reflectance study of Si-O vibrations in thermally treated alkalisaturated montmorillonites, Clay Miner. 34 (1999) 429–438.
[48] K.-I. Morigaki, A. Ohta, Analysis of the surface of lithium in organic electrolyte by atomic force microscopy, Fourier transform infrared spectroscopy and scanning auger electron microscopy, J. Power Sources. 76 (1998) 159–166.
[49] D. Aurbach, B. Markovsky, I. Weissman, E. Levi, Y. Ein-Eli, On the correlation between surface chemistry and performance of graphite negative electrodes for Li ion batteries, Electrochimica Acta. 45 (1999) 67–86.
[50] L.J. Radziemski, R. Engleman Jr., J.W. Brault, Fourier-transform-spectroscopy measurements in the spectra of neutral lithium, I6 and I7 (Li I), Phys. Rev. A. 52 (1995) 4462–4470.
[51] S. Brouillet-Fourmann, C. Carrot, N. Mignard, Gelatinization and gelation of corn starch followed by dynamic mechanical spectroscopy analysis, Rheol. Acta. 42 (2003) 110–117.
[52] S. Mathew, M. Brahmakumar, T.E. Abraham, Microstructural imaging and characterization of the mechanical, chemical, thermal, and swelling properties of starch-chitosan blend films, Biopolymers. 82 (2006) 176–187.
[53] F. Liu, B. Qin, L. He, R. Song, Novel starch/chitosan blending membrane: Antibacterial, permeable and mechanical properties, Carbohydr. Polym. 78 (2009) 146–150.
[54] F.A. López, A.L.R. Mercê, F.J. Alguacil, A. López-Delgado, A kinetic study on the thermal behaviour of chitosan, J. Therm. Anal. Calorim. 91 (2008) 633–639.
[55] N.L.G.D. Souza, H.M. Brandão, L.F.C. De Oliveira, Spectroscopic and thermogravimetric study of chitosan after incubation in bovine rumen, J. Mol. Struct. 1005 (2011) 186–191.
[56] M. Sugimoto, M. Morimoto, H. Sashiwa, H. Saimoto, Y. Shigemasa, Preparation and characterization of water-soluble chitin and chitosan derivatives, Carbohydr. Polym. 36 (1998) 49–59.
[57] J.R. Ferraro, Introductory raman spectroscopy, Academic press, 2003.
[58] H. Jantoljak, J.-P. Salvetat, L. Forró, C. Thomsen, Low-energy Raman-active phonons of multiwalled carbon nanotubes, Appl. Phys. Mater. Sci. Process. 67 (1998) 113–116.
[59] E.V. Efremov, F. Ariese, C. Gooijer, Achievements in resonance Raman spectroscopy. Review of a technique with a distinct analytical chemistry potential, Anal. Chim. Acta. 606 (2008) 119–134.
[60] X. Wang, C. Wang, L. Cheng, S.-T. Lee, Z. Liu, Noble metal coated single-walled carbon nanotubes for applications in surface enhanced raman scattering imaging and photothermal therapy, J. Am. Chem. Soc. 134 (2012) 7414–7422.
[61] R.Y. Sato-Berrú, E.V. Basiuk, J.M. Saniger, Application of principal component analysis to discriminate the Raman spectra of functionalized multiwalled carbon nanotubes, J. Raman Spectrosc. 37 (2006) 1302–1306.
[62] C. Thomsen, S. Reich, Raman scattering in carbon nanotubes, 2006.
[63] H. Kataura, Y. Achiba, X. Zhao, Y. Ando, Resonance Raman scattering of multi-walled carbon nanotubes, in: 2000: pp. 113–118.
[64] H. Athalin, S. Lefrant, A correlated method for quantifying mixed and dispersed carbon nanotubes: Analysis of the Raman band intensities and evidence of wavenumber shift, J. Raman Spectrosc. 36 (2005) 400–408.
[65] M.S. Dresselhaus, G. Dresselhaus, M. Hofmann, The big picture of Raman scattering in carbon nanotubes, Vib. Spectrosc. 45 (2007) 71–81.
[66] S. Gupta, R.J. Patel, Changes in the vibrational modes of carbon nanotubes induced by electron-beam irradiation: Resonance Raman spectroscopy, J. Raman Spectrosc. 38 (2007) 188–199.
[67] A. Jorio, R. Saito, G. Dresselhaus, M.S. Dresselhaus, Determination of nanotubes properties by Raman spectroscopy, Philos. Trans. R. Soc. Math. Phys. Eng. Sci. 362 (2004) 2311–2336.
[68] P. Delhaes, M. Couzi, M. Trinquecoste, J. Dentzer, H. Hamidou, C. Vix-Guterl, A comparison between Raman spectroscopy and surface characterizations of multiwall carbon nanotubes, Carbon. 44 (2006) 3005–3013.
[69] H.M. Heise, R. Kuckuk, A.K. Ojha, A. Srivastava, V. Srivastava, B.P. Asthana, Characterisation of carbonaceous materials using Raman spectroscopy: A comparison of carbon nanotube filters, single- And multi-walled nanotubes, graphitised porous carbon and graphite, J. Raman Spectrosc. 40 (2009) 344–353.

[70] M. Zdrojek, W. Gebicki, C. Jastrzebski, T. Melin, A. Huczko, Studies of multiwall carbon nanotubes using raman spectroscopy and atomic force microscopy, 2004.
[71] M.S. Dresselhaus, G. Dresselhaus, R. Saito, A. Jorio, Raman spectroscopy of carbon nanotubes, Phys. Rep. 409 (2005) 47–99.
[72] M.S. Dresselhaus, A. Jorio, A.G. Souza Filho, R. Saito, Defect characterization in graphene and carbon nanotubes using Raman spectroscopy, Philos. Trans. R. Soc. Math. Phys. Eng. Sci. 368 (2010) 5355–5377.
[73] D. Nishide, Y. Miyata, K. Yanagi, T. Tanaka, H. Kataura, PERIPUTOS: Purity evaluated by Raman intensity of pristine and ultracentrifuged topping of single-wall carbon nanotubes, Phys. Status Solidi B Basic Res. 246 (2009) 2728–2731.
[74] V.M. Irurzun, M.P. Ruiz, D.E. Resasco, Raman intensity measurements of single-walled carbon nanotube suspensions as a quantitative technique to assess purity, Carbon. 48 (2010) 2873–2881.
[75] H. Kataura, Y. Miyata, K. Mizuno, Purity and defect characterization of single-wall carbon nanotubes using raman spectroscopy, J. Nanomater. 2011 (2011).
[76] A.C. Dillon, M. Yudasaka, M.S. Dresselhaus, Employing Raman spectroscopy to qualitatively evaluate the purity of carbon single-wall nanotube materials, J. Nanosci. Nanotechnol. 4 (2004) 691–703.
[77] R.A. DiLeo, B.J. Landi, R.P. Raffaelle, Purity assessment of multiwalled carbon nanotubes by Raman spectroscopy, J. Appl. Phys. 101 (2007).
[78] R.P. Rocha, J.P.S. Sousa, A.M.T. Silva, M.F.R. Pereira, J.L. Figueiredo, Catalytic activity and stability of multiwalled carbon nanotubes in catalytic wet air oxidation of oxalic acid: The role of the basic nature induced by the surface chemistry, Appl. Catal. B Environ. 104 (2011) 330–336.
[79] X. Liu, R. Wang, L. Song, H. He, G. Zhang, X. Zi, et al., The oxidation of carbon monoxide over the palladium nanocube catalysts: Effect of the basic-property of the support, Catal. Commun. 46 (2014) 213–218.
[80] C. Ingrosso, G.V. Bianco, P. Lopalco, M. Tamborra, M.L. Curri, A. Corcelli, et al., Surface chemical functionalization of single walled carbon nanotubes with a bacteriorhodopsin mutant, Nanoscale. 4 (2012) 6434–6441.
[81] J. Zhao, A. Buldum, J. Han, J.P. Lu, First-principles study of Li-intercalated carbon nanotube ropes, Phys. Rev. Lett. 85 (2000) 1706–1709.
[82] G. Maurin, C. Bousquet, F. Henn, P. Bernier, R. Almairac, B. Simon, Electrochemical lithium intercalation into multiwall carbon nanotubes: A micro-Raman study, Solid State Ion. 136-137 (2000) 1295–1299.
[83] Y.A. Kim, M. Kojima, H. Muramatsu, S. Umemoto, T. Watanabe, K. Yoshida, et al., In situ Raman study on single- and double-walled carbon nanotubes as a function of lithium insertion, Small. 2 (2006) 667–676.
[84] G. Maurin, F. Henn, B. Simon, J.-F. Colomer, J.B. Nagy, Lithium Doping of Multiwalled Carbon Nanotubes Produced by Catalytic Decomposition, Nano Lett. 1 (2001) 75–79.
[85] J. Li, C. Wu, L. Guan, Lithium insertion/extraction properties of nanocarbon materials, J. Phys. Chem. C. 113 (2009) 18431–18435.
[86] J.T. Ye, Z.M. Li, Z.K. Tang, R. Saito, Raman spectra of lithium doped single-walled 0.4 nm carbon nanotubes, Phys. Rev. B - Condens. Matter Mater. Phys. 67 (2003) 1134041–1134044.
[87] A.K. Yoong, M. Kojima, H. Muramatsu, D. Shimamoto, T. Hayashi, M. Endo, et al., Raman study on electrochemical lithium insertion into multiwalled carbon nanotubes, J. Raman Spectrosc. 39 (2008) 1183–1188.
[88] M. Müller, R. Meinke, J. Maultzsch, B. Gebhardt, F. Hauke, A. Hirsch, et al., Resonant Raman scattering on carbon nanotubes covalently functionalized with lithium decyne, Phys. Status Solidi B Basic Res. 247 (2010) 2863–2866.
[89] A. Schechter, D. Aurbach, H. Cohen, X-ray photoelectron spectroscopy study of surface films formed on Li electrodes freshly prepared in alkyl carbonate solutions, Langmuir. 15 (1999) 3334–3342.
[90] K. Kanamura, S. Shiraishi, H. Takezawa, Z. Takehara, XPS analysis of the surface of a carbon electrode intercalated by lithium ions, Chem. Mater. 9 (1997) 1797–1804.
[91] D. Aurbach, I. Weissman, A. Schechter, H. Cohen, X-ray photoelectron spectroscopy studies of lithium surfaces prepared in several important electrolyte solutions. A comparison with previous studies by Fourier transform infrared spectroscopy, Langmuir. 12 (1996) 3991–4007.
[92] I. Ismail, A. Noda, A. Nishimoto, M. Watanabe, XPS study of lithium surface after contact with lithium-salt doped polymer electrolytes, Electrochimica Acta. 46 (2001) 1595–1603.
[93] M.E. Brown, P.K. Gallagher, Handbook of thermal analysis and calorimetry: Recent advances, techniques and applications, Elsevier, 2011.
[94] D.A. Skoog, F.J. Holler, T.A. Nieman, M. del C.M. Gómez, Principios de análisis instrumental, McGraw-Hill Madrid, 2001.
[95] Y.-J. Wu, L. Chao, K.-S. Ho, Y.-J. Huang, Y.-L. Huang, C.-S. Yang, et al., Characterizations on the amidized multiwalled carbon nanotubes grafted with polyaniline via in situ polymerization, J. Appl. Polym. Sci. 124 (2012) 5270–5278.
[96] A.A. Khiar, A.K. Arof, Conductivity studies of starch-based polymer electrolytes, Ionics. 16 (2010) 123–129.
[97] A.K. Arof, S. Amirudin, S.Z. Yusof, I.M. Noor, A method based on impedance spectroscopy to determine transport properties of polymer electrolytes, Phys. Chem. Chem. Phys. 16 (2014) 1856–1867.
[98] M.R. Johan, S. Ibrahim, Neural networks for Nyquist plots prediction in a nanocomposite polymer electrolyte (PEO–LiPF6–EC–CNT), Ionics. 17 (2011) 683–696.